Hydroxylamine Electrochemistry at Low-Index Single-Crystal Platinum Electrodes in Acidic Media

Victor Rosca, Guillermo L. Beltramo, and Marc T. M. Koper*

Schuit Institute of Catalysis, Laboratory of Inorganic Chemistry and Catalysis, Eindhoven University of Technology, 5600 MB Eindhoven, The Netherlands

Received: January 22, 2004; In Final Form: March 18, 2004

The electrochemistry of hydroxylamine at low-index single-crystal platinum electrodes in acidic media has been studied by voltammetry and in-situ FTIRRAS. Hydroxylamine (HAM) reactivity at platinum is largely controlled by interaction of the other components of the solution or products of the HAM partial oxidation with the electrode surface. Reduction of HAM is a structure-sensitive reaction, at least through the structure sensitivity of the hydrogen adsorption on platinum. No formation of gaseous products was detected in the potential region corresponding to the H_{upd} region on Pt(111) and Pt(110). Voltammetric and spectroscopic data point to adsorbed nitric oxide (NO) as the main stable intermediate of the HAM oxidation. Being electrochemically stable in a wide potential region between ca. 0.5 and 0.8 V, adsorbed NO acts as a poison for further oxidation of HAM. The HAM oxidation to NO appears to be a structure-insensitive process, though somewhat affected by the anion coadsorption. The Tafel slope analysis suggests the second electron transfer to be the rate-determining step in HAM oxidation to adsorbed NO. The mechanism of the HAM oxidation to NO_{ads} proposed here is consistent with the mechanism of the NO_{ads} reduction we have proposed elsewhere. Voltammetric data for all three low-index surfaces indicates the possibility of the HAM reduction and oxidation (at moderate potentials) to occur simultaneously. This fact may be tentatively explained by the existence of an intermediate, which appears both in the reduction and oxidation process. Accordingly, the reduction of HAM would be activated by a dehydrogenation step.

1. Introduction

Electrochemical transformations of hydroxylamine (HAM) are of great technological importance as well as of significant scientific interest. In industry, HAM is obtained by the liquid-phase catalytic hydrogenation of nitric oxide (NO) or nitrate at carbon-supported platinum or palladium catalysts.[1,2] The relevance of the electrochemical studies on similar catalysts as well as model systems for understanding the processes practiced in industry is well accepted.[3−6] From a scientific point of view, HAM electrochemistry is important for a fundamental understanding of the redox chemistry of inorganic nitrogen compounds. Furthermore, the electrochemical transformations of hydroxylamine could be attractive for studying fundamental aspects of multielectron/multiproton-transfer reactions.

The mechanisms of HAM oxidation and reduction on platinum are complex,[7] and only a limited number of detailed mechanistic studies have been reported so far.[8−14] The mechanism of HAM oxidation is commonly viewed in terms of stepwise dehydrogenation and further transformation of the intermediates. The intermediates of the first two electron−proton transfers in HAM oxidation (NOH and HNOH) are considered responsible for N_2O formation, either by their interaction on the surface or by their reaction with HAM in solution.[11−13] However, explicit evidence for these intermediates remains to be established. Other factors contributing to the complexity of the subject are (i) the adsorption of intermediates, products, and components of the electrolyte (anions, for example) on the electrode surface and (ii) the complex homogeneous chemistry of inorganic nitrogen containing compounds.

Recently, we have studied in detail the electrochemistry of HAM at polycrystalline platinum in acidic media, combining voltammetry, on-line mass spectrometry, and infrared spectroscopy.[13] An important conclusion was that the HAM electrochemical activity is effectively controlled by adsorption of other species, such as hydrogen, products of HAM oxidation (NO), anions (bisulfate), and other species. Under these circumstances, the investigation of the electrochemistry of HAM on platinum single-crystal electrodes is a logical next step, as the adsorption of these species on single-crystal surfaces is much better defined than on a polycrystalline surface. Studies on low-index single crystals may provide information on the structure sensitivity of the processes under investigation and help in resolving the effect of adsorption phenomena on the HAM reactivity.

Here, we present results of a combined voltammetric and infrared spectroscopic study of HAM electrochemistry at low-index single-crystal platinum electrodes in acidic media. Our aim was to characterize the reactivity of HAM on platinum and the effect of surface structure on the transformations of HAM. Fourier transform infrared absorption reflection spectroscopy (FTIRRAS) was used to detect two important products of HAM oxidation, nitric oxide (NO) and nitrous oxide (N_2O), as well as to identify the potential limits within which they are formed. We discuss the mechanistic aspects of HAM oxidation to NO and N_2O, as well as HAM reduction to ammonia. The mechanistic results are further discussed in light of our recent findings on the mechanism of the reduction of adsorbed NO (NO_{ads}) on polycrystalline platinum[15] and on a series of stepped Pt[n(111)×(111)] electrodes.[16]

* Address correspondence to this author. E-mail: M.T.M.Koper@tue.nl.

10.1021/jp049677p CCC: $27.50
Published on Web 05/25/2004

2. Experimental Section

The H_2SO_4 and $HClO_4$ working solutions were prepared from their respective concentrated acids ("Suprapur", Merck) and ultrapure water (Millipore MilliQ system, 18.2 MΩ cm, 2 ppb total organic carbon). The infrared experiments aimed at detection of nitric oxide and HAM were performed in a H_2SO_4 solution prepared with deuterium oxide (Merck, 99.8%). Hydroxylamine solutions were prepared by dissolving hydroxylammonium sulfate (Merck, "Pro Analysi") in ultrapure water or deuterium oxide. Prior to each experiment, all solutions were deoxygenated by purging with pure (N50) argon.

Bead-type single-crystal platinum electrodes, prepared by Clavilier's method,[17] were used for most of the electrochemical measurements. For the in-situ FTIR measurements, commercial platinum disk electrodes of 10 mm in diameter were used (Surface Preparation Laboratory, Zaandam, The Netherlands). Prior to each experiment, the working electrode was flame-annealed, cooled to room temperature in an $Ar:H_2$ (3:1) atmosphere, and transferred to the electrochemical cell under the protection of a droplet of deoxygenated ultrapure water.

Electrochemical measurements were performed in a conventional single-compartment three-electrode glass cell, using a computer-controlled potentiostat (AutoLab-PGSTAT20, Eco Chemie, Utrecht, The Netherlands). The cell and the other glassware were cleaned by boiling in a 1:1 mixture of concentrated nitric and sulfuric acid, followed by repeated boiling with ultrapure water. A coiled platinum wire served as counter electrode. In $HClO_4$ solutions, the reference electrode was an internal reversible hydrogen electrode (RHE). In H_2SO_4 solutions, a saturated mercury−mercury sulfate ($Hg/Hg_2SO_4/K_2SO_4$) electrode, connected via a Luggin capillary, was used as reference. However, all potentials are quoted versus the RHE.

The in-situ FTIRRAS measurements were performed under external reflection conditions. The spectrometer used was a Brüker IFS113V, equipped with a narrow-band MCT detector. The spectroelectrochemical cell[18] featured a prismatic CaF_2 window bevelled at 60°. To acquire FTIRAS data, 500 interferograms, at a resolution of 8 cm^{-1}, were collected at each potential. The reflectance spectra were calculated as $(R - R_0)/R_0$, where R and R_0 are the reflectance at the sample and the reference potential, respectively. Consequently, the $\Delta R/R$ ratio gives negative bands for species that are formed and positive bands for species consumed at the sample potential, as compared to the reference potential.

Prior to each experiment, the system cleanliness was checked by recording blank CV. The criteria for assessing the surface order and cleanliness of the electrode surface applied to electrodes used for in-situ IR measurements were identical to those practiced in our laboratory for purely electrochemical measurements.[19,20]

3. Results and Data Analysis

3.1. Pt (111). Figure 1A shows cyclic voltammograms (CVs) recorded at a Pt(111) electrode in contact with a HAM-containing sulfuric acid solution. To avoid any interference from the products of HAM oxidation, all potential sweep experiments were started in the hydrogen underpotential deposition (H_{upd}) region at about 0.07 V, unless otherwise stated, and subsequently ran in the positive direction (as also indicated by arrows). As can be seen from the figure, HAM shows no noticeable activity in the H_{upd} region up to ca. 0.2 V. However, above this potential, a prominent reduction peak occurs at ca. 0.3 V (E_{R4}^{111}), followed by the oxidation peak E_{O1}^{111} at ca. 0.45 V. The E_{R4}^{111} and E_{O1}^{111} features overlap partially, thus indicating that the corresponding processes are not completely separated on the potential scale. In contrast, the oxidation feature E_{O1}^{111} is well separated from the oxidation feature E_{O2}^{111} (at ca. 0.95 V) by a wide potential region of low positive current. If the positive-going potential sweep is reversed at 1 V, the only important voltammetric features observed in the negative-going sweep are the reduction peaks E_{R2}^{111} and E_{R3}^{111}. The situation is qualitatively similar in perchloric acid solution (Figure 1B), except for the higher current densities recorded in the positive-going sweep in the potential region between ca. 0.2 and 1 V for the latter electrolyte. This finding demonstrates the qualitative effect of anion adsorption, despite introducing small amounts of sulfate by using hydroxylammonium sulfate as the source of HAM.

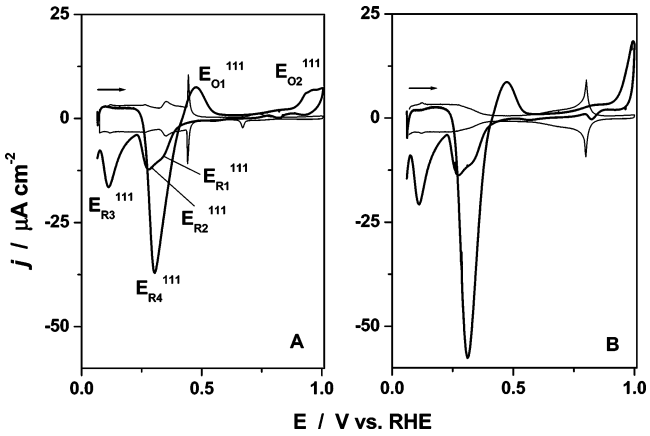

Figure 1. Cyclic voltammograms recorded at Pt(111) electrode in 0.5 M sulfuric (A) and 0.5 M perchloric (B) acid solutions in the absence (thin line) and presence (thick line) of hydroxylamine. Experimental conditions: 2.5×10^{-3} M NH_2OH; potential sweep rate 5 mV s^{-1}; starting potential 0.06 V.

The positive-going scan of the CV, presented in Figure 1A (or B), differs significantly from the negative-going one, presumably because of the formation, the blocking effect, and the reduction of some products of HAM oxidation. Continuous potential cycling, combined with a gradual increase of the upper potential limit of the CV, allowed us to follow the appearance and evolution of the reduction features E_{R2}^{111} and E_{R3}^{111} in the negative-going scan (see Figure 2). If a sufficiently low potential sweep rate is applied (5 mV s^{-1} or lower), the positive-going sweep has always the same shape, while the negative-going voltammetric profile changes as a function of the vertex potential. As shown in Figure 2A, the reduction features E_{R2}^{111} and E_{R3}^{111}, as well as the shoulderlike feature E_{R1}^{111}, appear and develop in the negative-going sweep with an increase of the upper potential limit of the corresponding CVs. Significantly, if the upper potential limit coincides with or is lower than the peak potential of the feature E_{R4}^{111}, no signs of the feature E_{R3}^{111} are present in the negative-going scan. Hence, in this potential region only HAM electroreduction should occur.

The CV profile observed can be understood in terms of (i) HAM reduction (E_{R4}^{111}), presumably to ammonia, which is the only possible reduction product, and (ii) HAM oxidation to nitric oxide (E_{O1}^{111}). The assumption of NO formation is based on a good match between both position and shape of the reduction features E_{R2}^{111} and E_{R3}^{111} with those observed for the reductive stripping of a NO adlayer under the same experimental conditions,[16] though in absence of HAM (Figure 2B, black and red lines). Furthermore, the Tafel slope analysis of the features E_{R2}^{111} and E_{R3}^{111}, carried out in $E_p - \log \upsilon$ coordinates,[21,22] gives slopes of 41 mV dec^{-1} and 142 mV dec^{-1}, respectively.

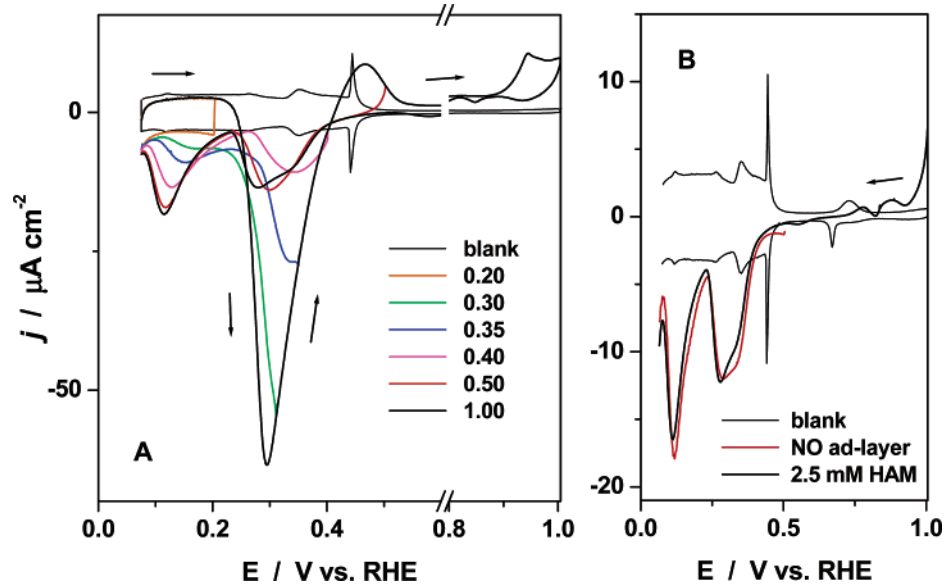

Figure 2. Cyclic voltammograms recorded at Pt(111) electrode in 0.5 M sulfuric (A). Numbers in the legend indicate the upper potential limit (vertex potential) of the corresponding CV. Experimental conditions: 5×10^{-3} M NH_2OH; potential sweep rate 5 mV s^{-1}. Starting potential 0.06 V. (B) presents a comparison of the negative-going voltammetric profiles recorded in the hydroxylamine containing solution and the NO adlayer stripping in the absence of hydroxylamine, as indicated in the legend.

These values are quite similar to those observed in the reductive stripping of the saturated NO adlayer, that is, 42 mV dec^{-1} and 126 mV dec^{-1}.[16] Because of the presence and stability of the NO adlayer, HAM oxidation is essentially blocked in a wide potential window between ca. 0.5 and 0.9 V. However, as will be argued below, in this potential region a slow (continuous) oxidation of HAM still takes place.

From the effect of the potential sweep rate on the peak height, it can be deduced that features E_{R2}^{111}, E_{R3}^{111}, and E_{O1}^{111} are all surface-confined processes. Their peak current densities show a linear increase with the potential sweep rate (in $\log j - \log v$ coordinates) in a wide window up to 1 V s^{-1}. The values of corresponding slopes were quite close to 1 (within 10% error). The linear regression analysis was applied to 6−10 experimental points and the square of the correlation coefficient (r^2) was at least 0.999 in all cases. The E_{R4}^{111} feature shows the same behavior (5 experimental points, slope 0.89, $r^2 = 0.997$), though in a narrow range of the sweep rate (2−20 mV s^{-1}), probably because of stronger overlapping with the feature E_{O1}^{111} at higher scan rate. An additional argument in favor of a surface reaction is provided by the applicability of the Langmuir adsorption isotherm to the corresponding process (see below).

The effect of the HAM concentration is analyzed on the basis of Figure 3A and 3B. We studied only moderate HAM concentrations (up to 50 mM), as in this range of concentrations the effect of anion adsorption could be easily followed. Figure 3A shows that (i) the reduction process corresponding to the feature E_{R4}^{111} is of positive order in HAM concentration and (ii) the oxidation process corresponding to the feature E_{O1}^{111} is of virtually zeroth order in HAM concentration. Additionally, an increase of HAM concentration results in an increase, although moderate, of the current density in the potential region between ca. 0.6 and 1 V, including the process corresponding to the feature E_{O2}^{111}. This observation supports the occurrence of the above-mentioned slow (continuous) HAM oxidation in this region in the presence of adsorbed NO, while the feature E_{O2}^{111} must be related to the oxidation of the NO adlayer to the adsorbed HNO_2 [23,24] and probably the reaction between the nitrite formed and HAM.

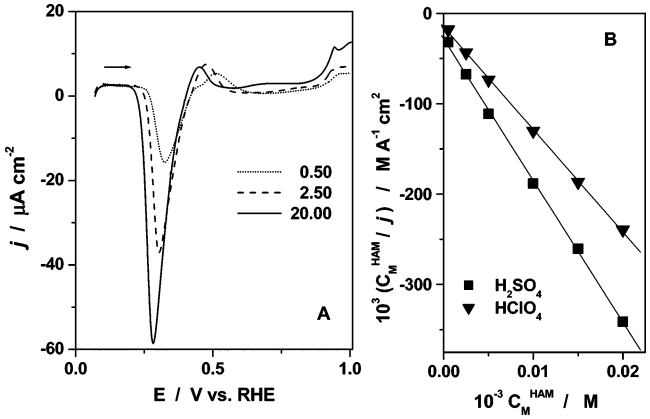

Figure 3. Effect of the hydroxylamine concentration on the positive-going voltammetric profile recorded at Pt(111) electrode (A) and the linearized Langmuir adsorption isotherm (B) (see text for details). Experimental conditions: 0.5 M H_2SO_4; potential sweep rate 5 mV s^{-1}; starting potential 0.06 V. Numbers in the legend of (A) indicate the hydroxylamine concentration in mM.

As shown above, the $\log j - \log v$ analysis of the feature E_{R4}^{111} suggests that the corresponding process of HAM reduction is a surface-confined process. Consequently, the current density (j) at a given potential should be proportional to the surface coverage of HAM (Θ_{HAM}). Under these circumstances, one can apply the Langmuir adsorption isotherm to test the hypothesis of adsorption. Here, we followed a simple formalism[25] that allows the linear form of the Langmuir adsorption isotherm to be used as a criterion for adsorption, although the procedure is of little use for estimating the HAM coverage. The final expression used was

$$(C_{HAM}/j) = 1/(k\,\beta_{HAM}) + (1/k) \times C_{HAM} \qquad (1)$$

where j is the observed current density (A cm^{-2}); C_{HAM} is the concentration of HAM (mol l^{-1}); k is the proportionality constant between the observed current density and the coverage of HAM[25] (A cm^{-2}); β_{HAM} is the adsorption parameter which also includes the activity coefficient (mol^{-1} l). Figure 3B shows the results of the graphic analysis on the basis of eq 1 (applied

potentials 0.3 V). From the figure, it can be seen that a good linearity was observed for experiments in both sulfuric and perchloric acid. The different values of the slopes reflect the effect of the specific adsorption of bisulfate.

So far, we have examined HAM electrochemistry at Pt(111) on the basis of voltammetry results. These results allowed us to identify adsorbed NO as an important intermediate of HAM oxidation. However, voltammetry is of little use for detection of another important product of HAM oxidation, that is, nitrous oxide (N_2O), which was observed by other authors[12] as well as in this laboratory[13] in studies with polycrystalline platinum.

In-situ FTIRRAS allows monitoring the consumption of HAM as well as the accumulation of the products and intermediates of its oxidation as a function of the applied potential, provided their characteristic spectroscopic features are well separated on the frequency axis. Bulk N_2O can be recognized by the asymmetric stretch (ν_1) band, centered at 2231 cm^{-1}.[26] The band displayed around 1460 cm^{-1} for the experiments in deuterium oxide was assigned to the −NOH (δ) bending mode in X_3NOH^+ (where X = H or D). This assignment is based on the theoretical values calculated with the Gaussian98 software package,[27−30] predicting a value of 1507 cm^{-1} for the −NOH (δ) bending mode in H_3NOH^+ and 1486 cm^{-1} in D_3NOH^+. Other possible vibration modes are well separated from the 1460−1500 cm^{-1} frequency range, as shown elsewhere (see Table 2 in ref 13). The band at ca. 1460 cm^{-1} is also observed in spectra for hydroxylammonium chloride.[31] On the other hand, if IR experiments are performed in normal water, ammonia in solution also contributes at wavenumbers around 1430 cm^{-1} (−(NH_3) (δ_s) mode in NH_4^+)[32] or even at somewhat higher frequencies (ca. 1460 cm^{-1} for ammonium perchlorate[33]). Consequently, for the experiments in normal water, it is difficult to discriminate between HAM and ammonia on the basis of the spectroscopic features around 1460 cm^{-1} alone. Turning now to NO, in principle, detection of adsorbed NO and NO in solution is possible. However, the assignment of the vibrational modes of adsorbed NO must be carried out with great care, as the N−O stretching mode will be displayed in a wide range of frequencies, depending on the surface orientation, NO coverage, and the applied potential.[34,35]

Figure 4 shows the potential difference IR spectra collected in experiments with the Pt(111) electrode. From these spectra, the consumption of HAM (Figure 4A) and formation of N_2O (Figure 4B) in the thin layer can be deduced. The potential dependent negative-going band displayed in the 1600−1700 cm^{-1} frequency range can be assigned to adsorbed NO. This assignment is in good agreement with previous studies of NO adlayers on Pt(111) under similar experimental conditions.[34,35] Furthermore, our experimental value of the "Stark-tuning" slope ($d\nu_{NO}/dE$) of 72 (±4) cm^{-1} V^{-1} lies in the range between 62 cm^{-1} V^{-1} and 85 cm^{-1} V^{-1}, reported by Weaver et al.[35] for the saturated (0.4−0.5) and subsaturated (0.3) NO coverage, respectively. Our CV data strongly suggest the formation of a nearly saturated NO adlayer, with a coverage around 0.4.

The integrated area of a given band presents a measure of the consumption or formation of the corresponding species in the thin layer, provided there is no significant depletion of these species from the thin layer during the data acquisition. Hence, by plotting the integrated area of the band versus applied potential, trends in HAM consumption and formation of NO and N_2O can be followed. Such a plot is shown in Figure 5. In all IR experiments, the upper potential limit was 0.9 V to avoid massive HAM depletion in the thin layer. From Figure 5 it can be concluded that HAM is consumed almost over the whole

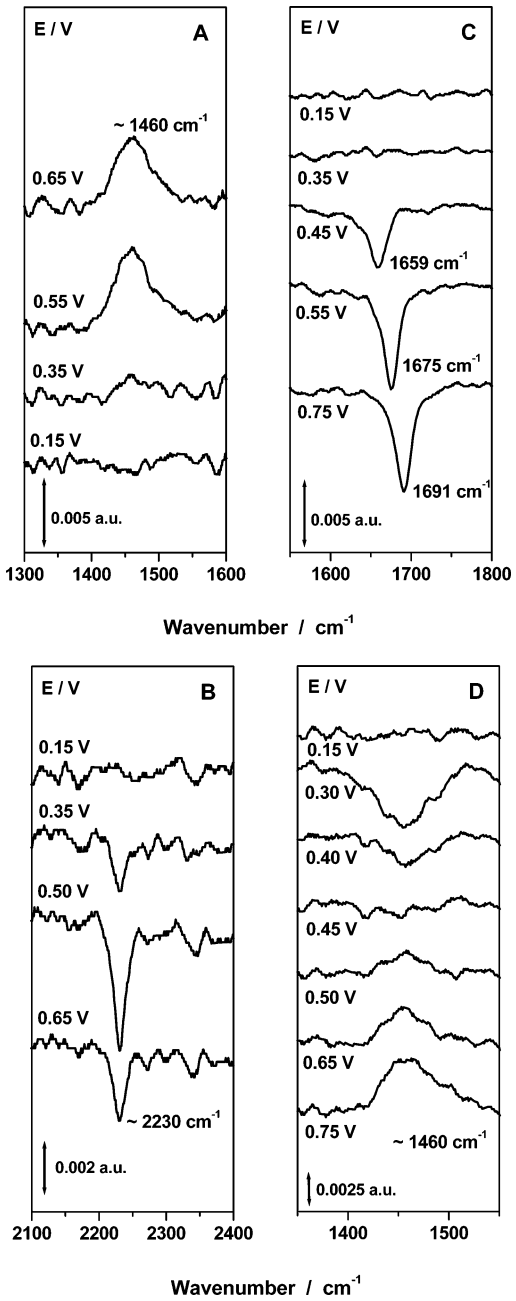

Figure 4. Potential difference FTIR spectra collected at Pt(111) electrode at different applied potentials (as indicated). Reference potential 0.1 V. Experimental conditions: 0.1 M H_2SO_4 + 1.5 × 10^{-2} M NH_2OH; in H_2O (B and D) and in D_2O (A and C); p, polarized light.

potential region examined. The leveling of HAM consumption between ca. 0.5 and 0.8 V may be related to the blocking effect of the NO adlayer, the formation of which was also deduced from the CV data. Significantly, for the same experiments in water a negative band (accumulation of species) was reproducibly observed around 1460 cm^{-1} (Figure 4D). The negative band appears in the potential region between ca. 0.2 and 0.4 V, that is, the potential region in which the voltammetric feature E_{R4}[111] occurs (Figure 1A), related to the reduction of HAM to ammonia. Since for the experiments in water the vibrational modes of both ammonia and hydroxylamine can contribute in the frequency range around 1460 cm^{-1}, the negative-going band may be caused by ammonia accumulation in the thin layer as a result of HAM reduction in the potential region between ca. 0.2 and 0.4 V. At higher potentials, a positive-going band

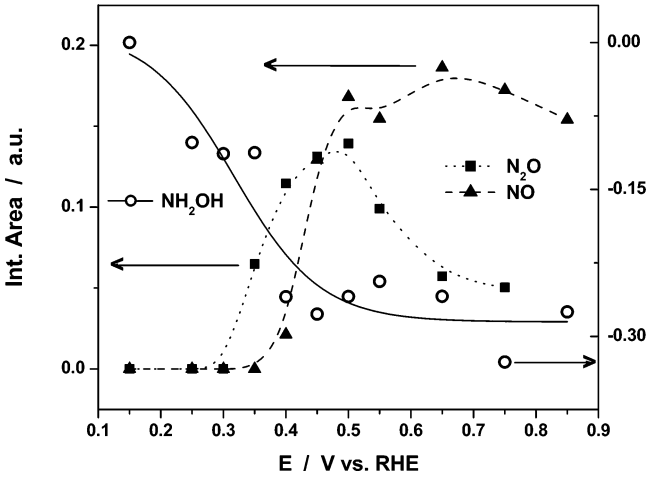

Figure 5. Trends in the hydroxylamine consumption and N_2O and NO_{ads} formation (as indicated in the legend) as a function of the applied potential. See also the text for details. Experimental conditions: as in Figure 4.

(consumption of species) emerges at around 1460 cm^{-1}, most probably related to HAM oxidation.

From Figure 5, it can also be seen that N_2O formation starts at ca. 0.3 V, its concentration in the thin layer increases up to ca. 0.5 V, and then it decreases with a tendency to level at around 0.7 V. The diffusion of N_2O out of the thin layer, in combination with a decrease of its formation rate between ca. 0.5 and 0.7 V, could account for the decrease of the integrated area of the corresponding band in this potential region. The potential region of increasing N_2O content coincides with the region where the processes corresponding to the voltammetric features E_{R4}^{111} and E_{O1}^{111} overlap (see Figure 2A). The curve corresponding to the NO band shows a sharp increase between ca. 0.4 and 0.5 V and a well-defined leveling in the potential region between ca. 0.5 and 0.9 V. This is in good agreement with the CV data, which points to the formation of a nearly saturated NO adlayer at above ca. 0.5 V. The trends of the curves shown in Figure 5 showed good reproducibility.

3.2. Pt (110). As shown in Figure 6A, the CV profile recorded at Pt(110) surface in contact with sulfuric acid is quite different from that recorded at Pt(111) under the same experimental conditions. Most significantly, the reduction peak at ca. 0.3 V observed at Pt(111) is not present. Furthermore, in contrast to the situation with Pt(111), at Pt(110) HAM shows reduction activity even at potentials corresponding to the saturation coverage of hydrogen (Figure 6A). On the other hand, similarly to Pt(111), a HAM oxidation wave to NO in the potential region between ca. 0.4 and 0.6 V can be readily deduced from the CV data. A gradual increase of the upper potential limit during continuous potential cycling brings about the appearance and development of the voltammetric features E_{R1}^{110} and E_{R2}^{110} in the subsequent negative-going sweep (Figure 6A). The increase of the upper potential limit from 0.4 to 0.6 V results in fully developed E_{R1}^{110} and E_{R2}^{110} peaks, showing that HAM reduction and oxidation processes occur simultaneously at potentials around 0.4 V. The negative-going part of the voltammetric profile recorded in the presence of HAM compares well with the one observed for the reductive stripping of the saturated NO adlayer (Figure 6B). However, in the presence of HAM the peak E_{R1}^{110} is less pronounced, probably because of a lower NO coverage resulting from HAM oxidation. The Tafel slope analysis of peaks E_{R1}^{110} and E_{R2}^{110} gave values of 39 mV dec^{-1} and 29 mV dec^{-1}, respectively. These values may be compared with 44 mV dec^{-1} and 42 mV dec^{-1}, respectively, obtained for the same features in the reductive stripping of NO adlayer.[16] The significant difference of the Tafel slope values in the E_{R2}^{110} feature is probably related to the presence of HAM.

The effect of the HAM concentration is examined from the positive-going linear sweep voltammograms (Figure 7) started in the H_{upd} region at ca. 0.06 V, to avoid interference from the products of HAM oxidation. As shown in Figure 7A and 7B, the reduction processes involving HAM in the potential region between ca. 0.06 and 0.4 V are of positive order in HAM concentration, while the oxidation process corresponding to the feature E_{O1}^{110} is of zeroth order in HAM concentration. Furthermore, as can be deduced from a comparison of the data presented in Figure 7A and 7B, the reduction processes in the potential region between ca. 0.06 and 0.4 V are significantly affected by the specific coadsorption of bisulfate, as expected for Pt(110). Additionally, the effect of the HAM concentration

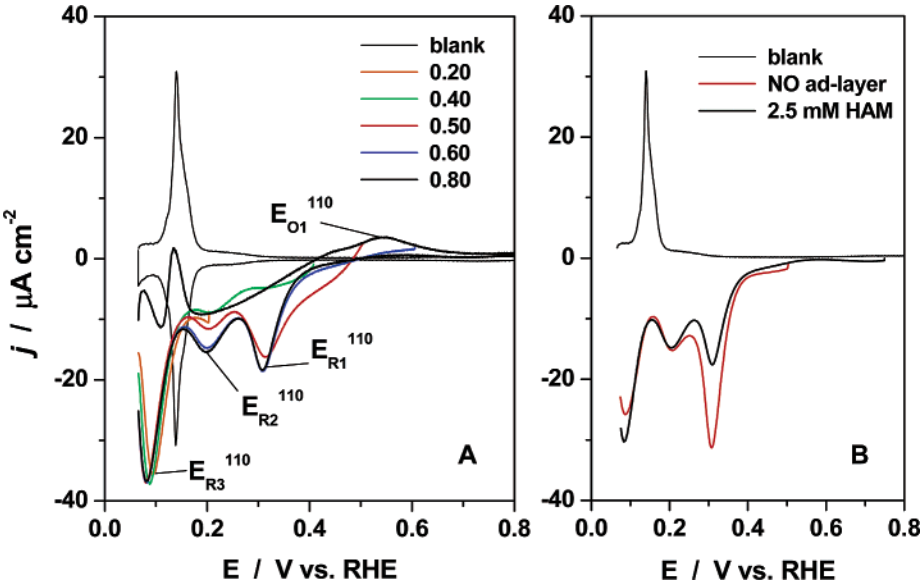

Figure 6. Cyclic voltammograms recorded at Pt(110) electrode in 0.5 M sulfuric (A). Numbers in the legend indicates the upper potential limit (vertex potential) of the corresponding CV. Experimental conditions: 5×10^{-3} M NH_2OH; potential sweep rate 5 mV s^{-1}. Starting potential 0.06 V. (B) a comparison of the negative-going voltammetric profile recorded at Pt(110) in the hydroxylamine containing solution and in the NO adlayer stripping in the absence of hydroxylamine, as indicated in the legend.

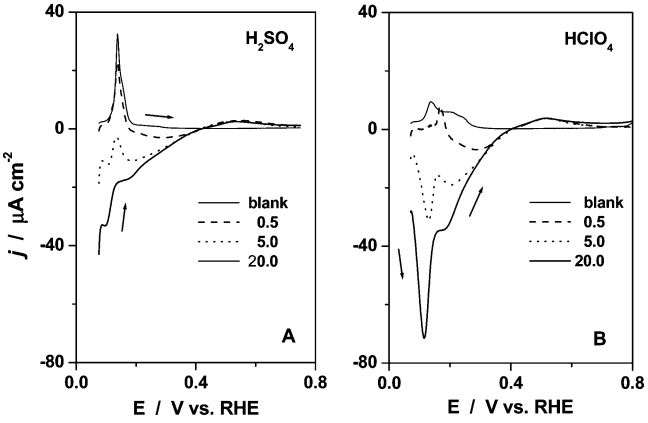

Figure 7. Effect of the hydroxylamine concentration on the positive-going voltammetric profile recorded at Pt(110) electrode in sulfuric acid (A) and perchloric acid (B). Numbers in legends indicate the hydroxylamine concentration in mM. Experimental conditions: 0.5 M H_2SO_4; potential sweep rate 5 mV s^{-1}; starting potential 0.06 V.

on the reduction processes under examination appears to be complex. At low concentrations (around 0.5 mM HAM), the positive-going potential sweep shows a minimum (Figure 7A and 7B, dashed lines), while further increase of the HAM concentration brings about a faster increase of the reduction current in the potential region below ca. 0.1 V. This complex trend is particularly well defined in the experiments in perchloric acid, where a prominent reduction peak can be observed at ca. 0.12 V. Interestingly, this potential value corresponds to a nearly saturated hydrogen coverage on Pt(110).

It is logical to assume that HAM reduction to ammonia is the process responsible for negative current in the potential region up to 0.4 V, since ammonia is the only possible HAM reduction product. At the same time, the effect of HAM concentration suggests that HAM reductive behavior could be more complex. Previously, we have reported a possible catalytic effect of HAM toward the hydrogen evolution reaction (HER),[13] as suggested from earlier mechanistic studies on HAM reduction on mercury electrodes.[36] By using on-line DEMS, we could observe a very small, though statistically significant, continuous increase of the *m*/*z* 2 (H_2) mass with increasing HAM concentration in 0.5 M H_2SO_4 solution in contact with polycrystalline platinum. Since the sites of the (110) plane are the dominating ones on polycrystalline platinum, the above-mentioned effect may occur on the well-oriented Pt(110) surface as well.

Examining the IR data for Pt(110) from the potential difference spectra given in Figure 8, HAM consumption (Figure 8A) as well as N_2O formation and accumulation (Figure 8B) in the thin layer can be deduced (in deuterated water). Figure 9, in which the corresponding integrated area versus potential curves are presented, shows that HAM is consumed over the whole potential range under examination (ca. 0.1−0.8 V) with a leveling between ca. 0.35 and 0.65 V, the potential region where the voltammetric feature E_{O1}^{110} is situated (see Figure 6A). Remarkably, for the same experiments in normal water, a positive band (consumption of species) at around 1460 cm^{-1} is observed as well (Figure 8D). This result is in contrast with the results for Pt(111), where a negative band (accumulation of species) is observed in the potential region between ca. 0.2 and 0.4 V. This observation can be tentatively explained by the lower current densities for HAM reduction at Pt(110) in sulfuric acid, as compared to Pt(111), and the considerably lower amounts of ammonia formed. Accordingly, in water the positive band (consumption of species) at around 1460 cm^{-1} may be

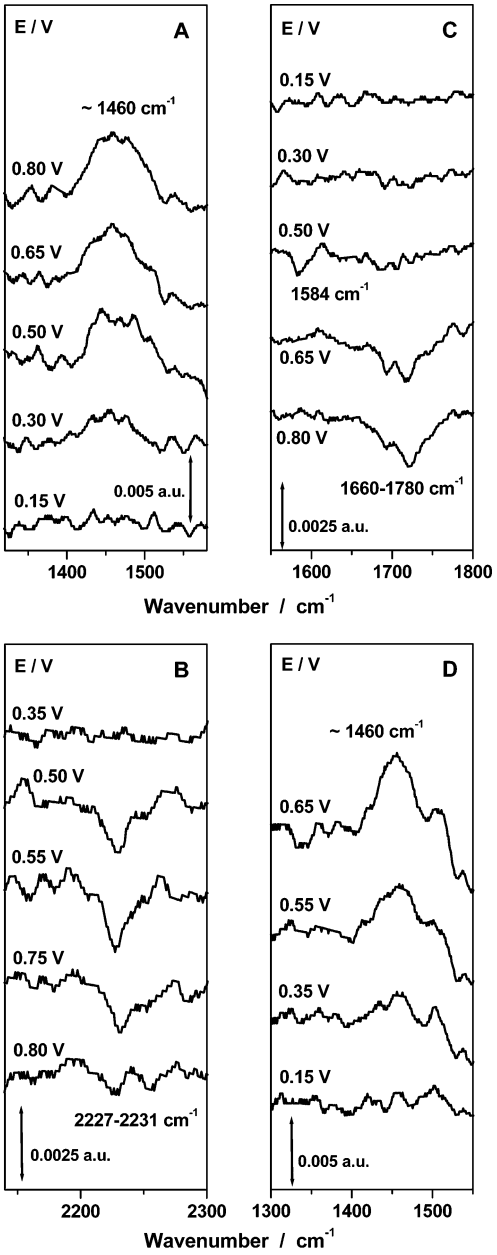

Figure 8. Potential difference FTIR spectra collected at Pt(110) electrode at different applied potentials (as indicated). Reference potential 0.1 V. Experimental conditions: 0.1 M H_2SO_4 + 1.5 × 10^{-2} M NH_2OH; in H_2O (B and D) and in D_2O (A and C); p, polarized light.

caused by a decrease of HAM concentration in the thin layer. As a final remark on the nature of the spectroscopic features around 1460 cm^{-1}, since this feature at least partially originates from an ionic solution species, the thin layer configuration may have a certain effect on the sign and evolution of the band as well. Figure 9 also shows that N_2O formation starts at around 0.4 V with a rise up to ca. 0.5 V, that is, in the potential region where the HAM oxidation to NO_{ads} takes place as well. It is difficult to argue about the further evolution of the trend for N_2O. However, N_2O formation is likely to be suppressed at higher (up to ca. 0.8 V) potentials as a result of filling up the NO adlayer and, consequently, blocking of the surface.

Figure 8C shows a series of spectra in the frequency range where features corresponding to N−O stretching vibrations in adsorbed NO are observed. The negative-going band centered at around 1584 cm^{-1} could be assigned to the bridge-bonded NO (low NO coverage), while a broad composite band between

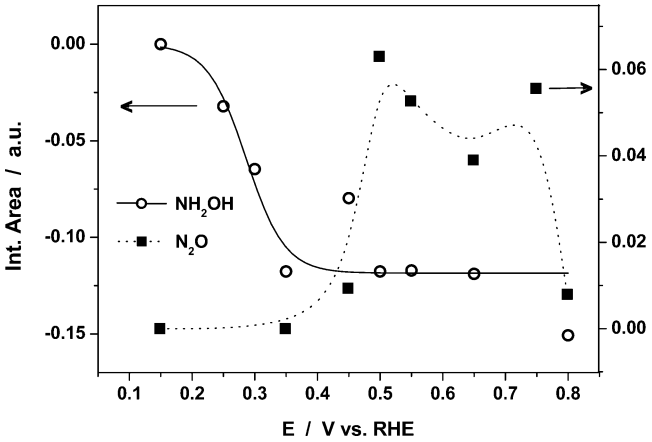

Figure 9. Trends in hydroxylamine consumption and N_2O formation (as indicated in the legend) as a function of the applied potential. See also the text for details. Experimental conditions: as in Figure 8.

ca. 1660 and 1780 cm^{-1} probably arises from N−O stretching of NO_{ads} in the atop position (intermediate to high NO coverage).[37] The following supports this assignment. First, the experiments with the s-polarized light showed the absence of any spectroscopic features in the 1600−1800 cm^{-1} region. Second, from experiments with NO adlayers on Pt(110) we could see a picture similar to that observed for HAM oxidation, that is, a broad (composite) negative-going band in the frequency region between ca. 1650 and 1800 cm^{-1} and a lower frequency band centered at ca. 1580 cm^{-1}.[38] Additionally, this assignment is in good agreement with results from the Alicante group. Gomez et al.[34] observed (i) a broad bipolar band at around 1740 cm^{-1} at near-saturation NO coverage and (ii) a weak bipolar band at ca. 1590 cm^{-1} at lower NO coverage in 0.1 M perchloric acid. A detailed IR analysis of the NO adsorption on Pt(110) is beyond the scope of this study. The spectroscopic data presented above provide sufficient evidence for the formation of a NO adlayer at potentials around 0.5 V and its increasing coverage at higher potentials as a result of the oxidation of HAM.

3.3. Pt (100). We shall start the presentation of the results for Pt(100) with the effect of concentration. As shown in Figure 10A, the positive-going potential sweep recorded in the experiments with Pt(100) surface in sulfuric acid is quite similar to that for Pt(111). First, Pt(100) does not show a significant activity toward HAM reduction in the potential region corresponding to a high coverage of hydrogen (0.06−0.25 V). Second, a prominent, concentration dependent, reduction peak (E_{R2}^{100}) is observed at subsaturated coverage of hydrogen. Third, the oxidation feature E_{O1}^{100}, corresponding most probably to HAM oxidation to adsorbed NO, occurs at ca. 0.5 V and is of zeroth order in HAM concentration, similarly to Pt(111). The formation of NO_{ads} can be deduced from the effect of HAM concentration on the negative-going sweep of the corresponding CVs (see Figure 10B). The height and position of the peak E_{R1}^{100}, which we attribute to the reductive stripping of the NO adlayer, increase with the concentration, pointing to a higher NO coverage achieved. The NO coverage approaches its saturation value at the highest concentration of the range examined (20 mM HAM), as deduced from the position of the E_{R1}^{100} peak. The peak is situated at ca. 0.24 V, a value quite close to 0.26 V observed by Rodes et al.[39] for the reductive stripping of a saturated NO adlayer in 0.1 M perchloric acid. An increase of NO coverage can be achieved by longer polarization at potentials above 0.6 V (up to 1000 s) at low concentrations as well. Finally, quite similar voltammetric profiles and trends were observed for similar experiments in perchloric acid.

The upper-potential test (see the Pt(111) section for details), performed in perchloric acid, revealed an interesting feature of the Pt(100) plane. As shown in Figure 11, in contrast to the Pt(111) plane, reversing the potential at values more negative than the position of the E_{R1}^{100} feature results in a significant reduction current in the negative-going scan, which cannot be associated with HAM reduction (see the curve reversed at 0.32 V). This observation points to the formation of a reducible product, despite the net reductive current in the positive-going sweep. The possible nature of this species is discussed in more detail in the Discussion section. Interestingly, increase of the upper potential limits up to ca. 0.65 V brings about formation of some NO_{ads} (feature E_{R1}^{100}). However, this increase does not have a significant effect on the negative-going voltammetric profile in the potential region between ca. 0.3 and 0.1 V under the experimental conditions considered (see the legend of Figure 11 for details). Further increase of the upper potential limit up

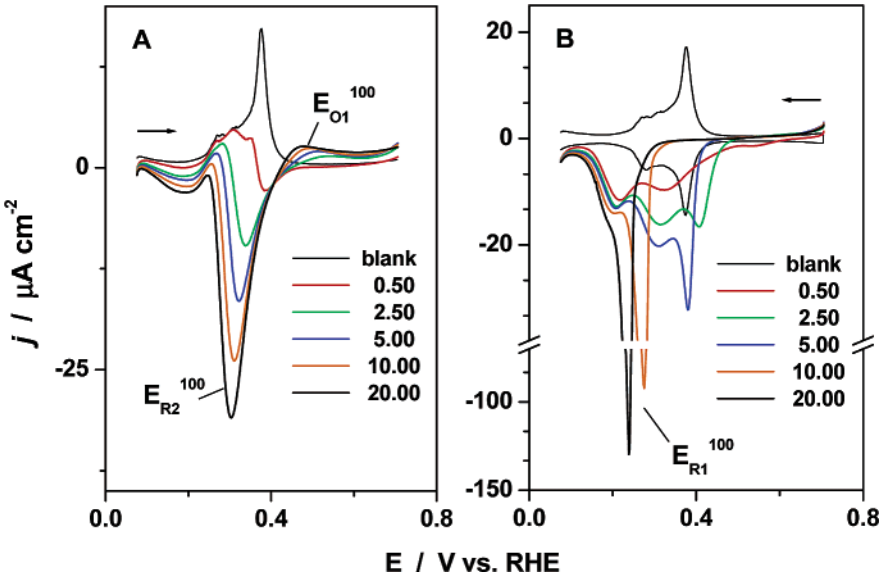

Figure 10. The positive-going (A) and the negative-going (B) part of the cyclic voltammograms recorded at Pt(100) electrode in 0.5 M sulfuric acid in the presence of hydroxylamine. Numbers in the legends indicate the hydroxylamine concentration in mM. Experimental conditions: potential sweep rate 5 mV s^{-1}; starting potential 0.06 V.

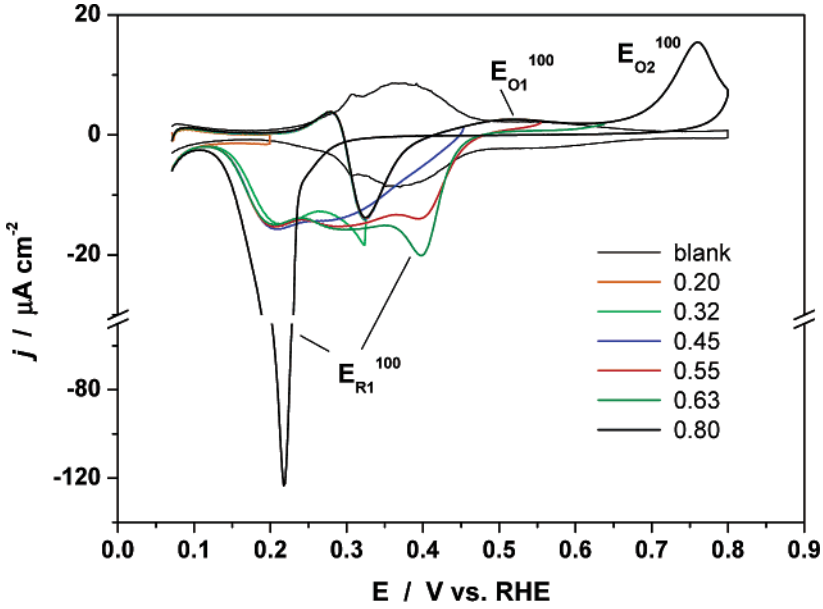

Figure 11. Cyclic voltammograms recorded at Pt(100) electrode in 0.5 M perchloric acid solution. Numbers in the legend indicate the upper potential limit (vertex potential) of the corresponding CV. Experimental conditions: 2.5×10^{-3} M NH_2OH; potential sweep rate 5 mV s^{-1}; starting potential 0.06 V.

to 0.8 V results in the oxidation feature E_{O2}^{100}, corresponding to the oxidation of adsorbed NO to nitrite[39] and a reaction between nitrite (and perhaps another product of NO oxidation) and HAM. The negative-going scan of the corresponding CV presents a sharp peak at ca. 0.22 V, thus indicating the formation of a (nearly) saturated NO adlayer in the positive-going scan.

3.4. Tafel Slope Analysis. The results of the Tafel slope analysis of HAM oxidation to NO on Pt(111) (feature E_{O1}^{111}, Figure 1A) and on Pt(110) (feature E_{O1}^{110}, Figure 6A) surfaces are presented in Figure 12A and Figure 12B, respectively. The analysis was performed in the peak potential versus logarithm of the sweep rate coordinates.[21,22] In Pt(111), the values of the Tafel slopes were 40 mV dec^{-1} and 38 mV dec^{-1} in sulfuric and perchloric acid, respectively. For the Pt(110) face, the value of the Tafel slope obtained from experiments in sulfuric acid was somewhat lower (33 mV dec^{-1}), though reasonably close to the value of 43 mV dec^{-1} for experiments in perchloric acid. A significant deviation from the theoretical value (40 mV dec^{-1}) of the Tafel slope was observed for the Pt(100) (Figure 10A, feature E_{O1}^{100}) in sulfuric acid (22 mV dec^{-1}, data not shown), while in perchloric acid no linearity was observed.

The results of the Tafel slope analysis suggest that the second electron transfer is the rate-determining step in the process of HAM oxidation to adsorbed NO, at least on Pt(111) and Pt-(110).

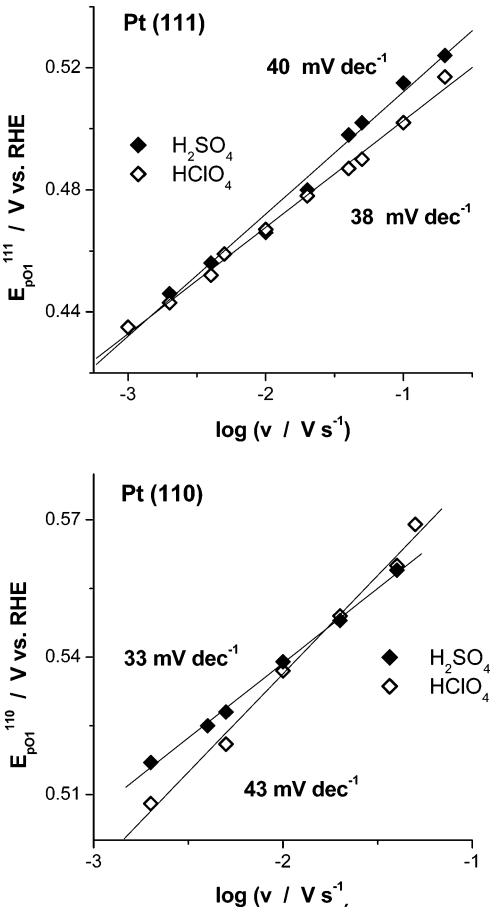

Figure 12. The Tafel slope analysis for the oxidation peaks E_{O1}^{111} (A) and E_{O1}^{110} (B) in 0.5 M sulfuric acid and 0.5 M perchloric acid, as indicated in the legend. Experimental conditions: 5×10^{-3} M NH_2OH; starting potential 0.06 V.

4. Discussion

We shall start the Discussion section with an analysis of the HAM oxidation. Voltammetric as well as spectroscopic data point to surface-bonded NO as the key intermediate in electrooxidation of HAM and not the adsorbed NOH (or HNO) intermediate as suggested in earlier studies.[12,14] Thus, this intermediate is assumed to be the main precursor for the formation of HNO_2, through a reaction with OH_{ads} species. In our experiments, the NO formation peak is observed at around 0.5 V on all surfaces examined. Furthermore, HAM oxidation is essentially blocked by the NO adlayer, which is stable over a relatively wide potential region (up to 0.7−0.9 V) depending on the surface orientation and the nature of the supporting electrolyte (perchlorate versus sulfate). The oxidation of the surface at higher potentials triggers oxidation of NO_{ads} and, consequently, further HAM oxidation. Recent studies of NO adlayers on single-crystal platinum electrodes provide sufficient (both voltammetric and spectroscopic) evidence for $HNO_{2(ads)}$ as the main product of the (reversible) oxidation of adsorbed

nitric oxide in the potential region between 0.9 and 1.1 V.[24,34,40] Therefore, it would be reasonable to accept this scenario for the oxidation of NO adlayers formed from the HAM containing solution. However, no reversibility of the surface-confined NO/HNO_2 is observed (Figures 1 and 11), most probably related to an irreversible reaction between HAM and surface HNO_2.

The Tafel slope analysis of the voltammetric peak corresponding to HAM oxidation to NO at low-index single-crystal platinum points to the second electron transfer as the rate-limiting step. This finding gives support to the tentative mechanism of HAM oxidation to NO_{ads}, proposed on the basis of our previous results on polycrystalline platinum:[13]

$$H_3NOH^+ \leftrightarrows H_3NOH_{ads}{}^+ \quad (2)$$

$$H_3NOH_{ads}{}^+ \leftrightarrows H_2NO_{ads} + 2H^+ + e^- \quad (3)$$

$$H_2NO_{ads} \rightarrow HNO_{ads} + H^+ + e^- \quad \text{rds} \quad (4)$$

$$HNO_{ads} \rightarrow NO_{ads} + H^+ + e^- \quad (5)$$

The HNO and H_2NO intermediates are suggested on the basis of their lower energy in vacuum compared to the NOH and HNOH species, as deduced from theoretical calculations[16,41] (the stability of the surface-bonded species is not known). In acidic media, the protonated HAM molecule is commonly perceived as the reactive species.[12,14,25] However, the exact nature of the reactive species in reaction 3 ($H_3NOH_{ads}{}^+$ vs H_2NOH_{ads}) should be considered as unknown, as the acid−base properties of HAM could be significantly affected upon interaction with the surface. Accordingly, reaction step 3 of HAM oxidation to NO may be tentatively split in two steps:

$$H_3NOH_{ads}{}^+ \leftrightarrows H_2NOH_{ads} + H^+ \quad (3')$$

$$H_2NOH_{ads} \leftrightarrows H_2NO_{ads} + H^+ + e^- \quad (3'')$$

The mechanism of HAM oxidation to NO_{ads} may be compared with the mechanism we have recently proposed for the reduction of NO_{ads}.[16] Briefly, the reductive stripping of the NO adlayer is perceived as a stepwise hydrogenation process, in which the formation of HNO and H_2NO intermediates is assumed:

$$NO_{ads} + H^+ + e^- \leftrightarrows HNO_{ads} \quad \text{equilibrium} \quad (6)$$

$$HNO_{ads} + H^+ + e^- \rightarrow H_2NO_{ads} \quad \text{rds} \quad (7)$$

$$H_2NO_{ads} + 4H^+ + 3e^- \rightarrow NH_4{}^+ + H_2O \quad \text{fast} \quad (8)$$

Ammonia is shown as the main product of the reduction of the adsorbed NO on platinum.[16,39] Importantly, the protons in reactions 6 and 7 seem to be transferred directly from a solution hydronium species.[16] Comparing schemes 2−5 and 6−8, reactions 4 and 7 are the forward and back reactions of the same transformation. At the same time, reactions 4 and 7 are the rate-determining steps in the reaction schemes 2−5 and 6−8, respectively. Consequently, the energetic barrier for the $HNO_{ads} \leftrightarrow H_2NO_{ads}$ transformation seems to be the highest in the whole $NO_{ads} \leftrightarrow NH_2OH$ chain of transformations, whatever the direction. The implication of these intermediates in the rate-determining step may indicate their relative stability and, thus, give a general explanation to occurrence of N−N condensation reactions during HAM oxidation and (continuous) NO reduction, resulting in formation of N_2O and N_2.

Another important issue to be considered is the formation of N_2O at moderately oxidative potentials. Spectroscopic data for Pt(111) and Pt(110) indicate formation of nitrous oxide starting at ca. 0.35 and 0.4 V, respectively. Since the maximum of the N_2O formation occurs in the potential region corresponding to subsaturated NO adlayer (ca. 0.45 V at Pt(111) and ca. 0.5 V at Pt(110)), a possible explanation would be an electrocatalytic reaction between adsorbed NO and HAM (or NO and products of HAM partial dehydrogenation), resulting in N−N condensation processes. This interpretation of the formation of N_2O (under potential control) is consistent with data on catalytic reaction between HAM and NO in acidic media at carbon-supported platinum catalysts, in which N_2O was shown as the product,[2] as well as with previous electrochemical studies on HAM oxidation on polycrystalline platinum.[12−14]

We shall continue the Discussion section with considering the HAM reductive activity. On Pt(111), the H_{upd} region is well separated from the bisulfate adsorption region, corresponding to the unique situation of an electrode surface almost free of hydrogen and anion adsorption. The prominent reduction peak, observed at about 0.3 V, that is, in the region of low hydrogen and bisulfate coverage, is a strong indicator of (i) high reductive activity of HAM on free platinum sites and (ii) strong dependence of HAM reductive activity on the surface interaction with hydrogen and anions. Interestingly, at the potential where HAM reduction starts in the positive-going sweep (ca. 0.20 V), the H_{upd} coverage is well below saturation, ca. 0.2 ML. This observation suggests that multiple adsorption sites (i.e., an "ensemble") are needed for HAM to be activated for reduction. The situation is quite similar for Pt(100) surface: HAM shows high reduction activity in the potential region between ca. 0.3−0.4 V, corresponding to subsaturated hydrogen and low bisulfate coverage. On Pt(110), the picture is somewhat different; HAM is reduced over the whole H_{upd} region, although affected by the nature of the anion. Furthermore, HAM is reduced even at potentials corresponding to high hydrogen coverage, suggesting that the Pt(110) surface nearly saturated with adsorbed hydrogen still exposes sites active for the activation of HAM reduction.

Before we proceed with a discussion of the mechanistic implications for HAM reduction, it would be interesting to briefly review previous mechanistic work on HAM reduction. In an early study of HAM reduction on bright platinum, Möller and Heckner interpreted their data in terms of hydrogen evolution.[8] In a later more detailed mechanistic study, the same authors assumed the breaking of the N−O bond in the first rate-determining step:

$$H_3NOH^+{}_{ads} + e^- \rightarrow (NH_3)_{ads} + (OH^{\bullet})_{ads} \quad (12)$$

In two subsequent steps, a fast electron transfer to and protonation of the adsorbed $OH^{\bullet}$ species is postulated. A low rate of HAM reduction was explained by the blocking effect of the adsorbed NH_3 species.[25] This mechanism raises several questions. First, HAM reduction is of positive order in respect to HAM concentration, as deduced from polycrystalline[13] as well as single-crystal studies (this work), which is inconsistent with blockage by $(NH_3)_{ads}$ species. Second, reaction 12 should perhaps consist of several elementary steps, which would allow understanding the mechanism of breaking the N−O bond in HAM.

An important clue in looking for an alternative scenario for HAM reduction on platinum may be the fact that at all surfaces examined the features corresponding to HAM reduction and

oxidation partially overlap (around 0.4 V), suggesting their simultaneous occurrence. This observation is in agreement with the platinum-catalyzed disproportionation of HAM resulting in ammonia and nitrous oxide (N_2O).[2] One possible explanation involves the assumption that the oxidation and reduction of HAM have a common intermediate. These considerations would lead us to the following tentative mechanism of HAM reduction:

$$H_3NOH^+ \leftrightarrows H_3NOH_{ads}{}^+ \qquad \text{equilibrium} \qquad (9)$$

$$H_3NOH_{ads}{}^+ \leftrightarrows H_2NO_{ads} + 2H^+ + e^- \qquad (10)$$

$$H_2NO_{ads} + 4H^+ + 3e^- \rightarrow NH_4{}^+ + H_2O \qquad (11)$$

Here, we assume that a possible way to activate reduction of HAM is partial dehydrogenation of the HAM (reaction 10) and formation of an adsorbed intermediate. Reactions 9 and 10 are identical to reactions 2 and 3, that is, the first two steps of the scheme proposed for HAM oxidation to NO_{ads}, leading to an intermediate (H_2NO_{ads}) which serves as a precursor to both $NH_4{}^+$ and NO_{ads} formation. In other words, the HAM reduction process contains an oxidative activation step—reaction 10. This reaction should require multiple adsorption sites, as also argued for HAM reduction on Pt(111) and Pt(100). In contrast to the mechanism proposed by Möller and Heckner, N−O bond is assumed to be broken at a later stage in the reaction.

Support in favor of the reaction scheme 9−11 is provided by the voltammetric data for Pt(100). The voltammograms in Figure 11 show a feature at ca. 0.22 V corresponding to reduction of a presumably adsorbed species. The position and shape of this feature is of zeroth order in HAM concentration (Figure 10B) and do not depend on the upper potential limit of the CVs (Figure 11) once the value of ca. 0.3 V is reached. Furthermore, the presence of the reduction feature at 0.22 V for all upper potential limits higher than 0.3 V suggests that it is related to the reduction of an intermediate of the NO reduction (or even NO itself). Accordingly, the adsorbate under consideration must be a compound in which nitrogen has formal oxidation state between (+2) and (−2) but it cannot be HAM, as the positive-going scan indicates that HAM cannot be reduced at these low potentials. A possible candidate is the adsorbed H_2NO (HNOH) intermediate. Regardless of our inability to exactly identify the nature of the species, we believe this observation gives some support in favor of an oxidative activation of HAM reduction.

Finally, let us comment on the structure sensitivity of the HAM reduction and oxidation in connection to its reactivity on polycrystalline platinum, as well as in connection to the structure sensitivity of related reactions such as nitrite reduction and methanol oxidation. Comparing the reduction activity on the low-index planes to polycrystalline platinum leads to the conclusion that the reactivity of polycrystalline platinum is dominated by sites of (110) orientation. The Pt(111) and Pt(100) surfaces are more active toward HAM reduction, but only in a limited potential region, which in Pt(111) is clearly related to very low coverage of hydrogen and anions on the surface. Interestingly, both Pt(111) and Pt(100) become completely blocked for HAM reduction by hydrogen coverages that are significantly below saturation; for Pt(111) the critical coverage below which the HAM reduction starts is ca. 0.2−0.3 ML. The same observation was recently made for nitrate reduction on Pt(111),[42] suggesting that both HAM and nitrate reduction need multiple adsorption sites (an "ensemble") to adsorb and react. More generally, these results indicate that for weakly adsorbed reactants, such as HAM and nitrate, the reactive sites are those sites where the competition with coadsorbates is the least dominant. Such sites typically tend to be (111) and (100) terrace sites. Comparing the HAM oxidation voltammetry on the three surfaces studied here suggests an insignificant structure sensitivity for HAM oxidation to NO_{ads}. This is in sharp contrast with the observed structure sensitivity of a very similar reaction, namely, methanol (MeOH) oxidation on platinum. Methanol oxidation is an order of magnitude faster on Pt(110) compared to Pt(111),[43] and recent chronoamperometric results indicate that methanol decomposition to adsorbed carbon monoxide takes place preferentially on the step sites of stepped platinum electrodes.[44] We assume that these differences between HAM and MeOH dehydrogenation kinetics may be traced back to their different adsorption strength.

5. Conclusions

In this paper, we have studied the electrochemistry of hydroxylamine at low-index single-crystal platinum electrodes in acidic media by voltammetry and in-situ FTIRRAS. We have focused particularly on the mechanistic aspects of HAM electrochemical transformations and the effect of the adsorption phenomena on the HAM reactivity on platinum.

Hydroxylamine electrochemistry at platinum is largely controlled by the interaction of the other components of the solution or products of the HAM partial oxidation with the electrode surface, such as adsorbed hydrogen, sulfate, and nitric oxide. Reduction of HAM seems to require multiple adsorption sites and is a structure-sensitive reaction, at least through the structure sensitivity of the hydrogen adsorption on platinum. No formation of gaseous products was detected in the potential region corresponding to the H_{upd} region on Pt(111) and Pt(110).

Voltammetric and spectroscopic data point to adsorbed NO as the main stable intermediate of the HAM oxidation. Being electrochemically stable in a wide potential region between ca. 0.5 and 0.8 V (dependent on the surface orientation and the nature of the supporting electrolyte), adsorbed NO acts as a poison for further oxidation of HAM. The HAM oxidation to nitric oxide appears to be a structure-insensitive process, though somewhat affected by the anion coadsorption. The Tafel slope analysis suggests the second electron transfer to be the rate-determining step in HAM oxidation to adsorbed NO.

The mechanism of the HAM oxidation to NO_{ads} proposed here is consistent with the mechanism of the NO_{ads} reduction we have proposed elsewhere.[16] Remarkably, the energetic barrier for the $HNO_{ads} \leftrightarrow H_2NO_{ads}$ transformation seems to be the highest in the $NO_{ads} \leftrightarrow NH_2OH$ chain of transformations, whatever the direction.

Voltammetric data for all three low-index surfaces indicate the possibility of the HAM reduction and oxidation (at moderate potentials) to occur simultaneously. This observation may be tentatively explained by the existence of an intermediate (H_2NO_{ads}), which appears both in reduction and oxidation of HAM, thus suggesting that HAM reduction is activated by an oxidative (dehydrogenation) step. The existence of a common intermediate in HAM reduction and oxidation would provide a natural explanation for the platinum-catalyzed disproportionation of HAM.

Acknowledgment. This work was supported by a grant from The Netherlands Organization for Scientific Research (NWO).

References and Notes

(1) Ritz, J.; Fuchs, H.; Perryman, H. G. Hydroxylamine. In *Ulmann's Encyclopedia of Industrial Chemistry*, 6th ed.; Wiley: Chichester, U.K., 2000.

(2) Moesdijk van de, C. G. M. The catalytic reduction of nitrite and nitric oxide to hydroxylamine: kinetics and mechanism. Ph.D. Thesis, Eindhoven University of Technology, 1979.

(3) Tauszik, G. R.; Grocetta, P. *Appl. Catal.* **1985**, *17*, 1.

(4) Gootzen, J. F. E. In-situ spectroscopic and electrochemical studies related to liquid-phase heterogeneous catalysis. Ph.D. Thesis, Eindhoven University of Technology, 1997.

(5) Savodnik, N. N.; Shepelin, V. A.; Zalkind, T. I. *Elektrokhimiya* **1971**, *7*, 583.

(6) Savodnik, N. N.; Shepelin, V. A.; Zalkind, T. I. *Elektrokhimiya* **1971**, *7*, 424.

(7) Plieth, W. J. Nitrogen. In *Encyclopedia of Electrochemistry of the Elements*; Bard, A. J., Ed.; Marcel Dekker: New York, 1978; Vol. 8, p 422.

(8) Moeller, D.; Heckner, K. H. *Z. Chem.* **1971**, *11*, 157.

(9) Moeller, D.; Heckner, K. H. *Z. Chem.* **1971**, *11*, 32.

(10) Moeller, D.; Heckner, K. H. *Z. Chem.* **1971**, *11*, 356.

(11) Moeller, D.; Heckner, K. H. *Z. Phys. Chem.* **1972**, *251*, 81.

(12) Karabinas, P.; Wolter, O.; Heitbaum, J. *Ber. Bunsen-Ges. Phys. Chem.* **1984**, *88*, 1191.

(13) Rosca, V.; Beltramo, G. L.; Koper, M. T. M. *J. Electroanal. Chem.* **2004**, *566*, 53.

(14) Piela, B.; Wrona, P. K. *J. Electrochem. Soc.* **2004**, *151*, E69.

(15) de Vooys, A. C. A.; Koper, M. T. M.; Santen van, R. A.; van Veen, J. A. R. *J. Electroanal. Chem.* **2001**, *506*, 127.

(16) Beltramo, G. L.; Koper, M. T. M. *Langmuir* **2003**, *19*, 8907.

(17) Clavilier, J.; Armand, D.; Sun, S. G.; Petit, M. *J. Electroanal. Chem. Interfacial Electrochem.* **1986**, *205*, 267.

(18) Iwasita, T.; Nart, F. C.; Vielstich, W. *Ber. Bunsen-Ges. Phys. Chem.* **1990**, *94*, 1030.

(19) Lebedeva, N. P.; Koper, M. T. M.; Herrero, E.; Feliu, J. M.; Santen van, R. A. *J. Electroanal. Chem.* **2000**, *487*, 37.

(20) Lebedeva, N. P.; Rodes, A.; Feliu, J. M.; Koper, M. T. M.; Santen van, R. A. *J. Phys. Chem. B* **2002**, *106*, 9863.

(21) Christiansen, P. A.; Hamnett, A. *Techniques and Mechanisms in Electrochemistry*; Blackie Academic and Proffessional: Glasgow, U.K., 1994.

(22) Koper, M. T. M.; Jansen, A. P. J.; Santen van, R. A.; Lukkien, J. J.; Hilbers, P. A. J. *J. Chem. Phys.* **1998**, *109*, 6051.

(23) Ye, S.; Kita, H. *J. Electroanal. Chem.* **1993**, *346*, 489.

(24) Zang, Z.-H.; Wu, Z.-L.; Yau, S.-L. *J. Phys. Chem. B* **1999**, *103*, 9624.

(25) Moeller, D.; Heckner, K. H. *Z. Phys. Chem.* **1974**, *255*, 33.

(26) Nakamoto, K. *Infrared and Raman Spectra of Inorganic and Coordination Compounds*; John Wiley & Sons: New York, 1986.

(27) Frisch, M. J.; Trucks, G. W.; Schlegel, H. B.; Scuseria, G. E.; Robb, M. A.; Cheeseman, J. R.; Zakrzewski, V. G.; Montgomery, J. A.; Stratmann, R. E.; Burant, J. C.; Dapprich, S.; Millam, J. M.; Daniels, A. D.; Kudin, K. N.; Strain, M. C.; Farkas, O.; Tomasi, J.; Barone, V.; Cossi, M.; Cammi, R.; Mennucci, B.; Pomelli, C.; Adamo, C.; Clifford, S.; Ochterski, J.; Petersson, G. A.; Ayala, P. Y.; Cui, Q.; Morokuma, K.; Malick, D. K.; Rabuck, A. D.; Raghavachari, K.; Foresman, J. B.; Cioslowski, J.; Ortiz, J. V.; Baboul, A. G.; Stefanov, B. B.; Liu, G.; Liashenko, A.; Piskorz, P.; Komaromi, I.; Gomperts, R.; Martin, R. L.; Fox, D. J.; Keith, T.; Al-Laham, M. A.; Peng, C. Y.; Nanayakkara, A.; Gonzalez, C.; Challacombe, M.; Gill, P. M. W.; Johnson, B. G.; Chen, W.; Wong, M. W.; Andres, J. L.; Head-Gordon, M.; Replogle, E. S.; Pople, J. A. *Gaussian 98*; Gaussian Inc.: Pittsburgh, PA, 1998.

(28) All reported harmonic vibrational frequencies were obtained from density functional (DFT) theory calculations using Gaussian 98 (ref 27). All species were fully optimized with Becke's three-parameter exchange functional (B3) (ref 29) and the Lee, Yang, and Parr (LYP) (ref 30) correlation functional, which includes both local and nonlocal terms as implemented in the Gaussian98 program package. For all atoms, 6-31G* basis sets have been used.

(29) Becke, A. D. *J. Chem. Phys.* **1993**, *98*, 5648.

(30) Lee, C.; Yang, W.; Parr, R. G. *Phys. Rev. B* **1988**, *37*, 785.

(31) Pouchert, C. J. *The Aldrich Library of Infrared Spectra*; Aldrich Chemical Co., Inc.: Milwaukee, WI, 1981.

(32) Silverstein, R. M.; Bassler, G. C.; Morrill, T. C. *Spectrometric Identification of Organic Compounds*; John Wiley & Sons: New York, 1991.

(33) Corrigan, D. S.; Weaver, M. J. *J. Electroanal. Chem.* **1988**, *239*, 55.

(34) Gomez, R.; Rodes, A.; Orts, J. M.; Feliu, J. M.; Perez, J. M. *Surf. Sci.* **1995**, *342*, L1104.

(35) Weaver, M. J.; Zou, S.; Tang, C. *J. Chem. Phys.* **1999**, *111*, 368.

(36) Heyrowsky, M.; Vavrichka, S. *Collect. Czech. Chem. Commun.* **1969**, *34*, 4, 1204.

(37) Brown, W. A.; King, D. A. *J. Phys. Chem. B* **2000**, *104*, 2578.

(38) Rosca, V.; Beltramo, G. L.; Koper, M. T. M., to be published.

(39) Rodes, A.; Climent, V.; Orts, J. M.; Perez, J. M.; Aldaz, A. *Electrochim. Acta* **1998**, *44*, 1077.

(40) Rodes, A.; Gomez, R.; Perez, J. M.; Feliu, J. M.; Aldaz, A. *Electrochim. Acta* **1996**, *41*, 729.

(41) de Vooys, A. C. A.; Koper, M. T. M.; van Santen, R. A.; van Veen, J. A. R. *Electrochim. Acta* **2001**, *46*, 923.

(42) Dima, G. E.; Beltramo, G. L.; Koper, M. T. M., manuscript in preparation.

(43) Herrero, E.; Franaszczuk, K.; Wieckowski, A. *J. Phys. Chem.* **1994**, *98*, 5074.

(44) Housmans, T. H. M.; Koper, M. T. M. *J. Phys. Chem. B* **2003**, *107*, 8557.